Marine Micropaleontology 175 (2022) 102156

Contents lists available at ScienceDirect

Marine Micropaleontology

journal homepage: www.elsevier.com/locate/marmicro

# Origin and evolutionary trends of the Neogene genera *Amaurolithus* and *Nicklithus* (calcareous nannofossils)

Carlos Lancis [a], José-Enrique Tent-Manclús [a,*], José-Abel Flores [b]

[a] University of Alicante, Department of Earth and Environmental Sciences, Apto. 99, 03080 San Vicente del Raspeig, Alicante, Spain
[b] University of Salamanca, Department of Geology, Plaza de la Merced s/n, 37008 Salamanca, Spain

ARTICLE INFO

*Keywords:*
Calcareous nannofossil evolution
Ceratoliths
*Amaurolithus*
*Nicklithus*
*Orthorhabdus*
Late Neogene
ODP Hole 999A
ODP Site 1237

ABSTRACT

Sediment samples from Ocean Drilling Program (ODP) Sites 999 and 1237 in the Caribbean Sea and Eastern Pacific Ocean were studied to monitor the evolution of ceratoliths from 7.4 Ma to 6 Ma. *Orthorhabdus rugosus* shows high variability at the end of the Tortonian to the Early Messinian (7.35 Ma to 6.91 Ma), resulting in the *Amaurolithus* (7.354 Ma) and *Nicklithus* branches (6.985 Ma). *Orthorhabdus rugosus* is an ortholith with three blades (sinistral, median, and dextral). The first ceratholith, *A. primus*, has two arms and a horseshoe shape with marked laths, and is stable and concave upwards. Its sinistral arm is formed from the sinistral blade of *Orthorhabdus rugosus* and the right arm is formed from the other blades. Early robust *A. primus* evolved into stylised forms and then to *Amaurolithus delicatus* (7.226 Ma), an almost plain horseshoe ceratolith with two arms. The left arm, usually the longer one, comes from the sinistral wing of *A. primus* and has a characteristic flattened omega section (Ω) without laths. There is a distribution overlap between *A. primus* and *A. delicatus*; the highest occurrence of the first one, at 6.282 Ma, is a newly proposed bioevent for the Messinian. After this, *Amaurolithus* does not have laths on its longer left arm and should be included in *A. delicatus*. The second branch has only one species, *Nicklithus amplificus*, which became extinct at 6.049 Ma. The dextral and median blades of *O. rugosus* form the *N. amplificus* dextral arm. The sinistral arm, which has the characteristic beak, hook, or hawk's bill, is the main difference between the development of this horseshoe and that of the previous one. The descriptions of *A. primus, A. delicatus*, and *N. amplificus* were specified based on the proposed evolutionary genesis.

## 1. Introduction

Horseshoe-shaped nannoliths, known as ceratoliths, are a characteristic Neogene group that is frequently used in calcareous nannofossil biostratigraphy at middle and low latitudes. The genus *Amaurolithus* Gartner and Bukry (1975) is a Late Neogene calcareous nannofossil included in the family Ceratolithaceae Norris, 1965 *emend* Young and Bown, 2014, derived from the genus *Ceratolithus* Kamptner (1950), the first described nannolith genera with a horseshoe form. Like coccolithophores, ceratolith-bearing cells are part of the calcifying unicellular algal group included in the Haptophyta division (Jordan and Chamberlain, 1997) where coccolithophores are included.

Norris (1965) showed that a single ceratolith is typically wrapped around the cell, and that beyond the ceratolith, a large coccosphere of hoop-shaped coccoliths sometimes occurs. Alcober and Jordan (1997), Young et al. (1999), Cros et al. (2000), and Sprengel and Young (2000) observed *Ceratolithus cristatus* hoop-shaped coccoliths inside coccospheres of *Neosphaera coccolithomorpha* planoliths, suggesting that ceratoliths, planoliths, and hoop coccoliths may form during alternate phases of a complex life cycle; thus, *N. coccolithomorpha* is a synonym of *C. cristatus*. The *Neosphaera*-phase planoliths show typical heterococcolith features; hence, a likely hypothesis is that the ceratolith stage is equivalent to the holococcolith stage in other taxa and thus haploid (Young et al., 2005). Some coccospheres, such as *Umbilicosphaera sibogae*, include up to four cells (Young et al., 2003). However, molecular genetic data and culture observations are not yet available.

Traditional fossil coccolithophore taxonomy was established using the morphological characteristics of coccoliths (and/or nannoliths) preserved in the sedimentary record (Tappan, 1980; Perch-Nielsen, 1985), based on the crystallographic orientation of the crystal unit components (Young, 1998). This taxonomy has been successfully applied to fossil records and compares well with characterisation methods of modern coccolithophores, such as cell ultrastructure, life cycles, and, more recently, molecular genetics (Cros et al., 2000; Geisen

* Corresponding author.
*E-mail addresses:* Carlos.lancis@ua.es (C. Lancis), je.tent@ua.es (J.-E. Tent-Manclús), flores@usal.es (J.-A. Flores).

https://doi.org/10.1016/j.marmicro.2022.102156
Received 19 November 2021; Received in revised form 30 June 2022; Accepted 7 July 2022
Available online 11 July 2022

et al., 2002; Saez et al., 2003).

High-resolution studies in continuous well-dated sedimentary sections of oceanic boreholes have demonstrated morphological changes occurring over time in species of some groups across wide geographic areas, which has stimulated researchers interested in evolutionary trends: e.g. Bukry (1971), Haq (1973), Romein (1979), Theodoridis (1984), Aubry (1988), Raffi et al. (1998), Young (1990), Blaj et al. (2010), Bord (2013), Monechi et al. (2013), Ciummelli and Raffi (2013), Blair et al. (2017), Bergen et al. (2017), Boesiger et al. (2017), Browning et al. (2017), and De Kaenel et al. (2017).

Gartner and Bukry (1975) addressed the phylogeny of the Ceratolithaceae family. Raffi et al. (1998) described the evolutionary lineages of ceratoliths and also define the genus *Nicklithus*. Alternatively, Young and Bown (2014) included the genera *Triquetrorhabdulus* and *Orthorhabdus in the family*.

The present work focuses on the phylogenetic links among the genera *Orthorhabdus, Amaurolithus*, and *Nicklithus*, with specific documentation of their origin and temporal distribution, as well as their taxonomy. The study is based on detailed fossil content in continuous sedimentary sections from the Ocean Drilling Program (ODP) Sites 999 and 1237 (Sigurdsson et al., 1997; Mix et al., 2003), with highly abundant, well-preserved, and diverse calcareous nannofossils.

## 2. Material and methods

### 2.1. Oceanographic setting

ODP Hole 999A was obtained during the ODP Leg 165 in the western Colombian Caribbean Basin, at 12°44.639′N, 78°44.360′W, at a water depth of 2827.9 m, on a promontory informally named Kogi Rise elevated nearly 1000 m above the relative flat Colombian Plain. The Kogi Rise was outside the influence of turbidite deposition in the Magdalena Fan complex (Sigurdsson et al., 1997) (Fig. 1A and B). Detailed site locations, core recoveries, and lithological descriptions can be found in Sigurdsson et al. (1997). The Upper Miocene interval consists of clayey nannofossil mixed sediment with foraminifers and interbedded ash layers, which are massive and structureless (Sigurdsson et al., 1997).

ODP Site 1237 was drilled during ODP Leg 202 and is located at 16°0.421′S, 76°22.685′W, in a water depth of 3212 m, on a relatively flat bench on the easternmost flank of the Nazca Ridge, approximately 140 km off the coast of Peru (Fig. 1A and C). The eastern Nazca Ridge is covered by a thick drape of pelagic sediment that extends to its shallowest reaches. The site comprises four holes, 1237A, 1237B, 1237C, and 1237D, integrated in the Site 1237 composite section (Mix et al., 2003). Detailed site locations, core recoveries, and lithological descriptions can be found in Mix et al. (2003). The entire drilled sequence is dominated by biogenic components, with a minor terrigenous (probably eolian) component that decreases downhole (Mix et al., 2003).

### 2.2. Sample preparation

A total of one hundred and two smear slides were prepared from Hole 999A between 224.58 mcd (metres corrected depth) and 180.59 mcd and 42 from Hole 1237B between 179.67 mcd and 113.53 mcd (see Annex 1), in the Department of Geology of the University of Salamanca using the decantation technique of Flores and Sierro (1997), being the focus of our study. In addition, 35 smear slides from Hole 999A obtained between 182 mcd and 151 mcd and 44 samples from Hole 1237 B obtained between 115 mcd and 7.76 mcd were checked to find *Amaurolithus* (Annex 1). The common spacing between the samples was 1 m, which decreased to 0.1 m in selected intervals. The slides were observed with a polarised microscope (PM) at X1000. To determine the fine details of the nannofossil structures, 21 samples from Hole 999A, three from 1237D, and seven from 1237C were prepared for the scanning electron microscopy (SEM) using a technique of centrifugation/filtration. The samples were disaggregated, using hydrogen peroxide and an ultrasound bath, before centrifugation to increase the silt/clay ratio. The preparation was then filtered using a vacuum pump, which concentrated the calcareous nannofossils in order to obtain clean samples. Then, 25 samples of Hole 999A and 53 of Site 1237 (Annex 1) of the Late

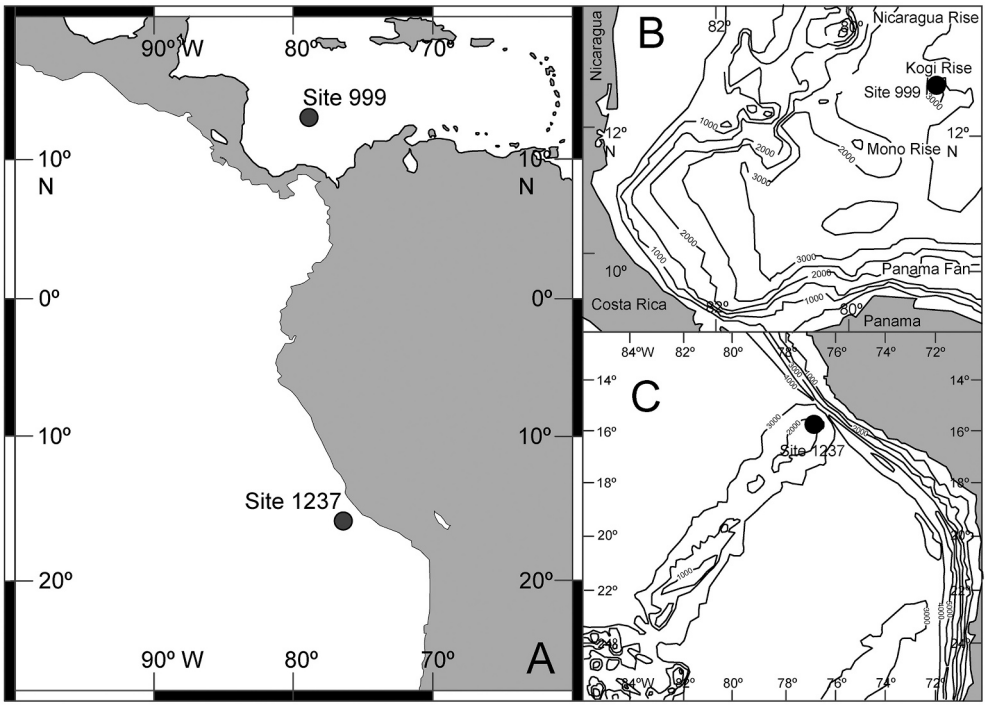


**Fig. 1.** A. Location map of ODP Sites: 999 drilled during Leg 165 (Sigurdsson et al., 1997) and 1237 drilled during Leg 202 (Mix et al., 2003); B. Bathymetric map (500-m contour interval) showing the location of Site 999 and the surrounding major features of the western Colombian Basin. Site 999 is located on the Kogi Rise 150 km northeast of the Mono Rise. C. Bathymetric map (1000-m contour interval) showing the location of Site 1237.

Messinian-Pliocene were checked using the SEM to determine the highest occurrence of *Amaurolithus*.

## 3. Biostratigraphy and biochronology

For Hole 999A, the age model was constructed using the orbitally-tuned $\delta^{18}O$ and $\delta^{13}C$ isotope records obtained from foraminifera (Bickert et al., 2004) with the considerations proposed by Kameo and Bralower (2000) and Buitrago-Reina et al. (2010) and the scales of Raffi et al. (2006) and Gradstein et al. (2012) (Table 1 and Fig. 2).

For ODP Site 1237, the biochronology and magnetostratigraphy is not well constrained for the interval between 8.9 Ma to 6 Ma (Mix et al., 2003). The bioevents of Hole 999A found in this study (Table 1) permitted the construction of an age model for the site (Table 2 and Fig. 2). The adjustment for the interval between 6 Ma and 2.5 Ma was calibrated astronomically and by benthic foraminifera isotopes (Tiedemann and Mix, 2007; Tiedemann et al., 2007).

## 4. Morphologies of ortholiths and ceratoliths

The specific terminology for the asymmetrical horseshoe-shaped form of ceratoliths was first established by Kamptner (1954) and complemented by Gartner and Bukry (1975), Perch-Nielsen (1985), and Aubry (1988). The family Ceratolithaceae includes horseshoe-shaped ceratoliths and three-bladed ortholiths (Fig. 3). The three-blades of the ortholiths have laths mainly perpendicular to the blade union, with the longer part in a centred portion but slightly displaced, and two pointing ends, one more acute than the other. The most pointed part is drawn up and described as the anterior side and the other the posterior side. The two more extended blades of *O. rugosus*, nearly in the same plane, allows the most stable positions with the median blade pointing up. This is the preferred orientation of the ortholith for PM preparations; the left blade is the sinistral blade (shown in blue in the figures), the right blade is the dextral blade (green in the figures), and the median blade points up (in red, Fig. 3A). This view is the upper face view (ufv) and the bottom face view (bfv) is shown when the median blade faces down (Fig. 3B).

The three blades of the ortholiths were modified to yield ceratoliths; therefore, the same terminology was used. Wings (as they have laths and arrowhead forms) are used to refer to the former blades, left as sinistral (blue), right as dextral (green), and median (red). The posterior pointed lath-ends of the left wing form a notch that evolves into the arch. The right arm is composed of joined dextral and median wings, and the latter forms a dentate keel. *Amaurolithus primus, A. delicatus*, and *N. amplificus* have three wings and two horseshoe arms (Fig. 3C–K). In the most stable orientation for the PM slides or the upper face view (ufv), these taxa do not show birefringence. The slight brightness observed in some specimens may be due to diagenetic overgrowth, which can tilt the horseshoe.

*Amaurolithus primus* has laths in the sinistral wing that bend towards the observer (Fig. 3C), and the posterior margin is straight (Fig. 3D) or slightly bent backwards. The sinistral wing of *A. delicatus*, usually the longer arm, is unrodded and has a characteristic flattened omega (Ω) cross section (Fig. 3G). It has an arch and a delicate dentate keel (red), and a spur and velum (green) (Fig. 3E–H). The sinistral wing of *N. amplificus* has both margins bent backwards, the anterior just slightly (Fig. 3I), and the lath-end folding upwards and to the posterior part, producing the characteristic hook, beak or hawk's bill on the posterior side (Fig. 3I–K). The robust dentate keel shows significant development (Fig. 3I). The dextral arm has a bifurcated end (Fig. 3J).

**Table 1**
Calcareous nannofossil events of the ODP Hole 999A used in the age-model.

| EVENT | CORE-SECTION-CM | Metres Corrected Depth | AGE Ma from Bickert et al., 2004 |
|---|---|---|---|
| HO. *N. amplificus* | 20H-3-45-**20H-3-70** | 181.71–**181.93** | 6.042–**6.049** |
| HO. *A. primus* | 21H-1-120-**21H-1-145** | 189.27–**189.41** | 6.277–**6.282** |
| HO *R. rotaria* | 21H-4-5-**21H-4-20** | 192.20–**192.33** | 6.422–**6.426** |
| LO. *N. amplificus* | **23**×-**3-80**-23×-3-145 | **204.02**–204.61 | **6.985**–6.992 |
| LO *A. delicatus* | **23**×-**7-40**-24×-1-5 | **209.06**–210.35 | **7.226**–7.288 |
| LO. *R. rotaria* | **24**×-**1-5**-24×-1-15 | **210.35**–210.44 | **7.288**–7.295 |
| LO *A. primus* | **24**×-**1-90**-24×-1-105 | **211.12**–211.25 | **7.354**–7.366 |

HO: Highest occurrence; LO: Lowest occurrence. The age was obtained after the calibrated depth versus age of the site obtained by Bickert et al. (2004). The event samples are indicated in bold font and the lower/upper samples in the LO/HO. The metres corrected depth (mcd) of each sample and the early/late calibrated ages are also shown.

## 5. Evolutionary patterns within the Ceratolithaceae

Gartner and Bukry (1975) published a major revision of the Ceratolithaceae. Bukry (1979), Perch-Nielsen (1985), Aubry (1988), Raffi et al. (1998), and Blair et al. (2017) added new species. The Nannotax 3.0 database includes the genera *Amaurolithus*, *Triquetrorhabdulus*, *Orthorhabdus*, and *Ceratolithus* (Young et al., 2022, Ceratholithaceae). The *Amaurolithus* and *Nicklithus* horseshoes observed with the PM show slight brightness or non-birefringence with crossed nicols, whereas *Ceratolithus* shows high birefringence (Kamptner, 1954; Gartner and Bukry, 1975; Raffi et al., 1998).

The evolutionary history of the ceratolith group traditionally follows Gartner's (1967) hypothesis of a relationship between *Amaurolithus* and *Orthorhabdus rugosus* as ancestral. Gartner and Bukry (1975) suggested a possible lineage within the ceratolith group and established a phylogenetic relationship considering *A. primus* the ancestral forms, questioning the liaison between *Triquetrorhabdulus* (herein named *Orthorhabdus* after Young and Bown, 2014) and *Ceratolithus/Amaurolithus*. They considered a monophyletic origin for the group, including *Ceratolithus*, the first form of which, *Ceratolithus acutus* (=*Ceratolithus armatus*), derived from *A. amplificus*.

However, Raffi et al. (1998) proposed an origin for the ceratolith structure derived from *O. rugosus* (*Triquetrorhabdulus rugosus* in their study). They documented three developments that produced different and successful branching: 1) the *A. primus* branch at the end of the Tortonian, 2) the *N. amplificus* branch during the Early Messinian, and 3) the *C. armatus* branch at the Messinian/Pliocene boundary. These authors observed intermediate forms between *O. rugosus, Orthorhabdus extensus*, and *O. finifer* (Theodoridis, 1984) and ceratoliths just below and across the first appearance of *A. primus, N. amplificus*, and *C. acutus* (=*C. armatus*), which illustrate the evolutionary transitions. These studies were based mainly on the observation of affinities using exclusively optical PM images.

## 6. *Orthorhabdus rugosus* ancestor of the horseshoe ceratoliths

Based on the samples studied, we observed two main *O. rugosus* variability episodes (Fig. 4): 1) at the end of the Tortonian to the Early Messinian and 2) at the end of the Messinian to the Early Pliocene. The first interval coincides with the LO of *Amaurolithus* and *Nicklithus* between 7.35 Ma and 6.91 Ma (Lourens et al., 2004); the second matches the LO of *Ceratolithus*, at approximately 5.35 Ma (Lourens et al., 2004).

In the first interval, the median blade (red) of *O. rugosus* hardly varies, so evolutionary change takes place in the two more extended blades, sinistral (blue) and dextral (green). During the second period, the *O. rugosus* median blade experienced the greatest modification, growth, and rotation to develop the dextral arm.

The species *O. extensus* (variable width of the two extended blades) and *Orthorhabdus striatus* (development of longitudinal ridges), based on

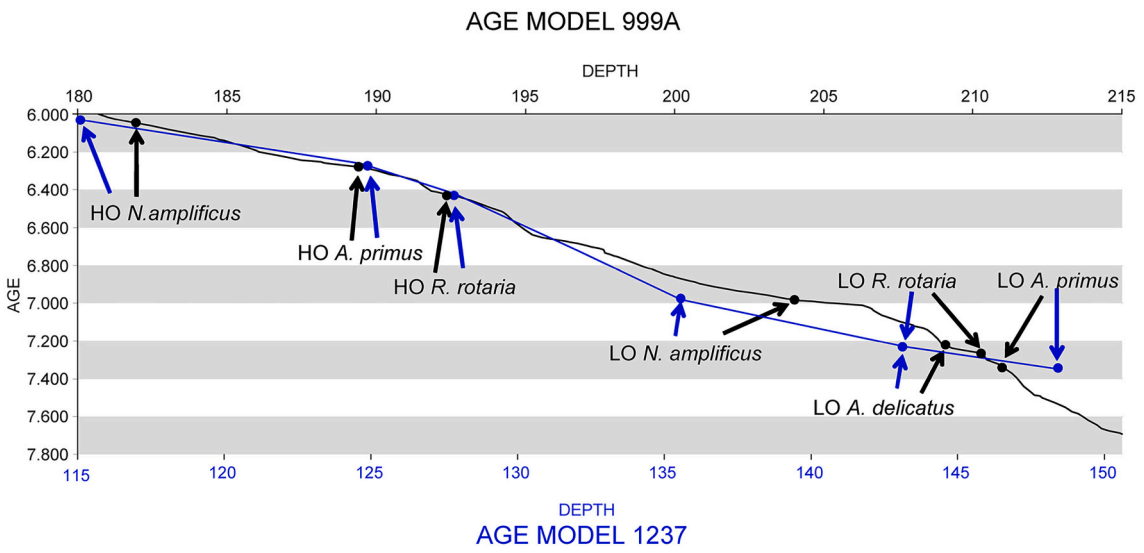


**Fig. 2.** Adopted age model of ODP Hole 999A (black) and 1237 (blue). Age model of 999A after Bickert et al. (2004). Composite age model of Site 1237 after Mix et al. (2003) showing the corrected depth (m) versus age (Ma) calculated in this study. (For interpretation of the references to colour in this figure legend, the reader is referred to the web version of this article.)

**Table 2**
Calcareous nannofossil events of the Site 1237 composite used for the calibration of the age model shown in Fig. 2.

| EVENT | CORE-SECTION-CM | Corrected Depth mbsf | AGE Ma |
|---|---|---|---|
| HO. *N. amplificus* | 1237B 12H 2–75-**1237B 12H 3–75** | 113.53–**115.04** | 6.042–**6.049** |
| HO. *A. primus* | 1237B 13H 2 75-**1237B 13H 3–75** | 123.34–**124.84** | 6.277–**6.282** |
| HO *R. rotaria* | 1237B 13H 4–75-**1237B 13H 5–75** | 126.34–**127.85** | 6.422–**6.426** |
| LO. *N. amplificus* | **1237B 14H 3–95**-1237B 14H 4–95 | **135.22**–136.72 | **6.985**–6.992 |
| LO *A. delicatus* | **1237B 15H 2–75**-1237B 15H 3–75 | **143.81**–145.32 | **7.226**–7.288* |
| LO. *R. rotaria* | **1237B 15H 2–75**-1237B 15H 3–75 | **143.81**–145.32 | **7.226**–7.288* |
| LO *A. primus* | **1237B 15H 6–75**-1237B 16H 1 75 | **149.86**–151.95 | **7.354**–7.366 |

The event samples are indicated in bold font and the lower/upper samples in the LO/HO. The metres corrected depth (mcd) of each sample and the early/late calibrated ages are also shown. *As both events coincide in the same sample the younger age has been used (mbsf: metres below sea floor).

observations with the PM, can be assigned to the variability of *O. rugosus*, as observed in the SEM images, in agreement with Raffi et al. (1998), or they could be broken forms of *A. primus* and/or *N. amplificus* (Fig. 4).

These observations are consistent with the provenance of *Amaurolithus* and *Nicklithus* from the *Orthorhabdus* specimens. They originate from a significant morphological change affecting the sinistral blade laths (the major blade) in different ways. The dextral blade was bent to the bottom portion of both genera. In contrast, in *Nicklithus*, the dentate keel (from the median blade) becomes higher and more robust (Fig. 3).

The HO of *O. rugosus* in the 999A is in the sample 999A 18H-1 W-145 (5.299 Ma).

## 7. The origin of *Amaurolithus primus*

The sudden appearance of *A. primus* in the sedimentary record at around 7.35 Ma was observed in both studied sections (Tables 1 and 2). Blair et al. (2017) advanced their first record at 7.559 Ma at ODP Site 926 by observing *A. primus*-like forms with the PM. Lancis (1998) mentioned *A. primus*-like forms prior to the first appearance of the species. Raffi et al. (1998) considered these 'unsuccessful attempts'. These *A. primus*-like forms have also been found at Site 1237, and in agreement with the last cited work, should be studied further.

Fig. 5 shows the set modifications of *O. rugosus* producing the early *A. primus*.

The modifications are not a gradual evolutionary sequence of intermediate progressively modified forms but occur simultaneously as they are present from the beginning of the first recorded specimens. *Amaurolithus primus* coexisted with the *O. rugosus* ancestor in the studied samples.

Figs. 6 and 7 illustrate the variability in *A. primus*. The initial forms are quite simple, but they show all the features defining the species (Fig. 6A–F) and the later specimens show a decreasing number of sinistral wing laths and curved to the posterior portion, developing a more pronounced arch (Fig. 7J–O). Occasionally, the loss of the lath anterior portion of the sinistral wing produces a clear spur (Fig. 6 M–O). These specimens have been named *A. tricorniculatus*, although we consider that they do not have enough differences from *A. primus* to be considered a different species. Our observations indicated a trend of increasing diversity with more stylised forms, maintaining the initial robust forms (Fig. 7E–H). The presence of marked laths on the sinistral wing is characteristic of *A. primus* throughout its distribution.

The last observed forms of *A. primus* (sinistral wing with laths) appear in samples 999A 21H 1 W-145 (at 6.282 Ma; Bickert et al., 2004) and 1237B 13H 3–75. In Hole 999A and Site 1237, in the younger samples studied (Annex 1), the *Amaurolithus* corresponds to the short morphotype without laths, with the flattened omega section of the sinistral wing, left arm (blue), included in the *A. delicatus* morphology (Fig. 8 and Fig. 9D, E, F, G, H, I, K, and N).

## 8. The origin of *Amaurolithus delicatus*

The first appearance of *A. delicatus* was recorded in samples 999A 23×-7-40 (at 7.226 Ma) and 1237B 15H-2-75. No intermediate forms were observed between *A. primus* and *A. delicatus*.

In the definition of *A. delicatus* species, Gartner and Bukry (1975) mentioned that '*A. delicatus* is no doubt closely related to *A. primus*, with which it may be associated throughout its range'. Gartner and Bukry (1975) suggested a possible ecologic relation 'as in many samples only one of the two species is present'. According to Raffi et al. (1998),

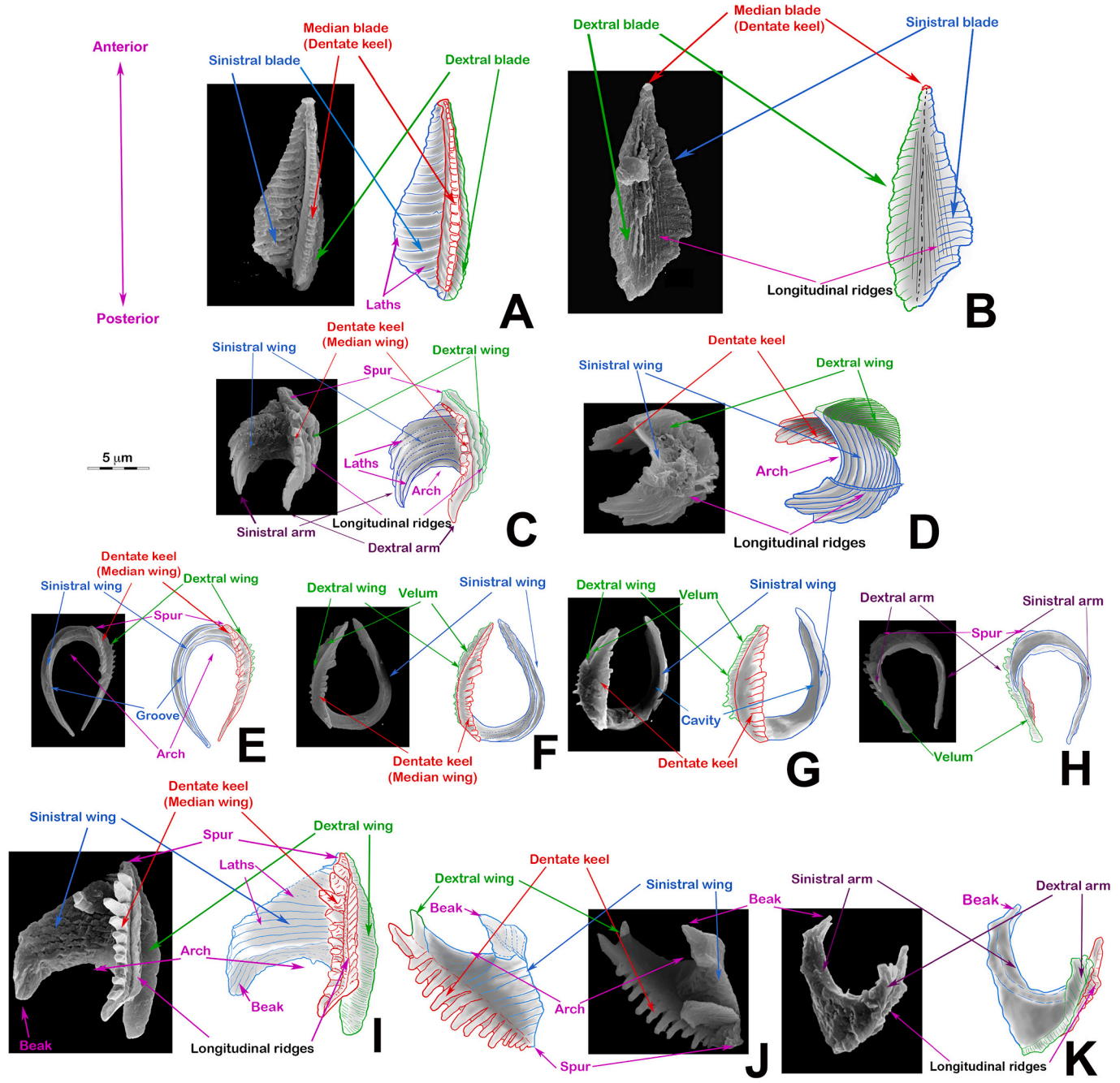


**Fig. 3.** Terminology of the ortholith *O. rugosus* and the ceratoliths *A. primus*, *A. delicatus*, and *N. amplificus*. A) *O. rugosus* ufv; B) *O. rugosus* bfv with longitudinal ridges; C) *A. primus* ufv; D) *A. primus* bfv; E) *A. delicatus* ufv; F) *A. delicatus* ufv; G) *A. delicatus* lateral ufv; H) *A. delicatus* bfv; I) *N. amplificus* ufv; J) *N. amplificus* lateral ufv; K) *N. amplificus* ufv.

*A. primus* may have given rise to three new species, *A. delicatus, A. bizarrus*, and *A. tricorniculatus*, which could be evidenced by the common shape, delicate construction, and optical behaviour of the four species.

Fig. 8 shows a proposed set of morphological changes in *A. primus* that could lead to the first *A. delicatus*: elongation of both wings, loss their laths on the sinistral wing, horseshoe-form thickness reduction, and sinistral wing flattened omega (Ω) cross-section development.

The sudden appearance in the fossil record of *A. delicatus* after *A. primus*, without intermediate forms, suggests that these changes occurred at the same time. Stylised *A. primus* was observed at the same time; later, *A. delicatus* appeared for the first time (Fig. 8). Fig. 9 illustrates the variability in *A. delicatus*.

Within the morphologic variability of the species, it is possible to observe stylised forms with all the features described (Fig. 9 A–C, J, and L) to shorter forms that classically have been included in *A. primus* morphology (Fig. 9G–I), but they have the type characteristics of *A. delicatus*, as they do not show laths. Blair et al. (2017) included roughly equidimensional narrow arcs and rounded *Amaurolithus* specimens in *A. brevigracilis* that could be included in *A. delicatus* variability. Other short specimens with pronounced spurs, named *A. tricorniculatus* (Fig. 9D–F), should be included within the variability of *A. delicatus*.

Alternatively, within the variability of *A. delicatus*, a set of robust forms with a thicker arch and more or less marked spur, as shown in Fig. 9K and N, have been named *A. ninae*.

*Amaurolithus delicatus* ranged from the bottom of the Messinian 7.226 Ma (sample 999A 23×-7–40) to the Pliocene, when it became

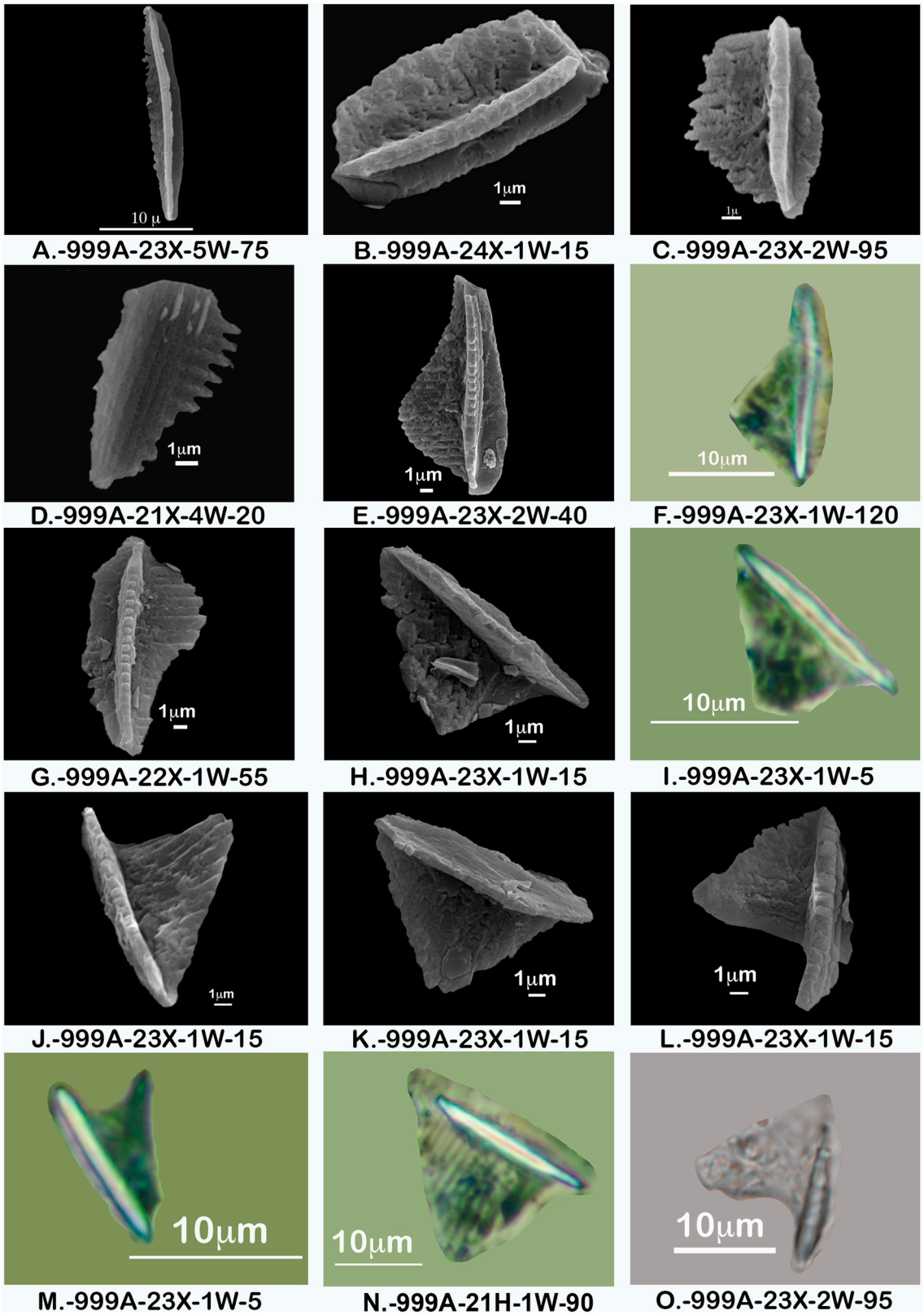


**Fig. 4.** Morphological variability in *O. rugosus* and broken *N. amplificus.* A to C, E and G: *O. rugosus* (SEM), all upper face view (ufv); F: *O. rugosus* obtained with the Polarised Microscope (PM) parallel nicols (PN), ufv equivalent to the E; D: *O. rugosus* (SEM) in bottom face view (bfv) form *O. striatus*. H, J, K, and L: broken *N. amplificus* (SEM, ufv); M, N, O, and I: equivalent respectively to the upper (J, K, L), or left (H) ones (PM, ufv), usually classified as *O. extensus*. Note the slight variations in the scale bars.

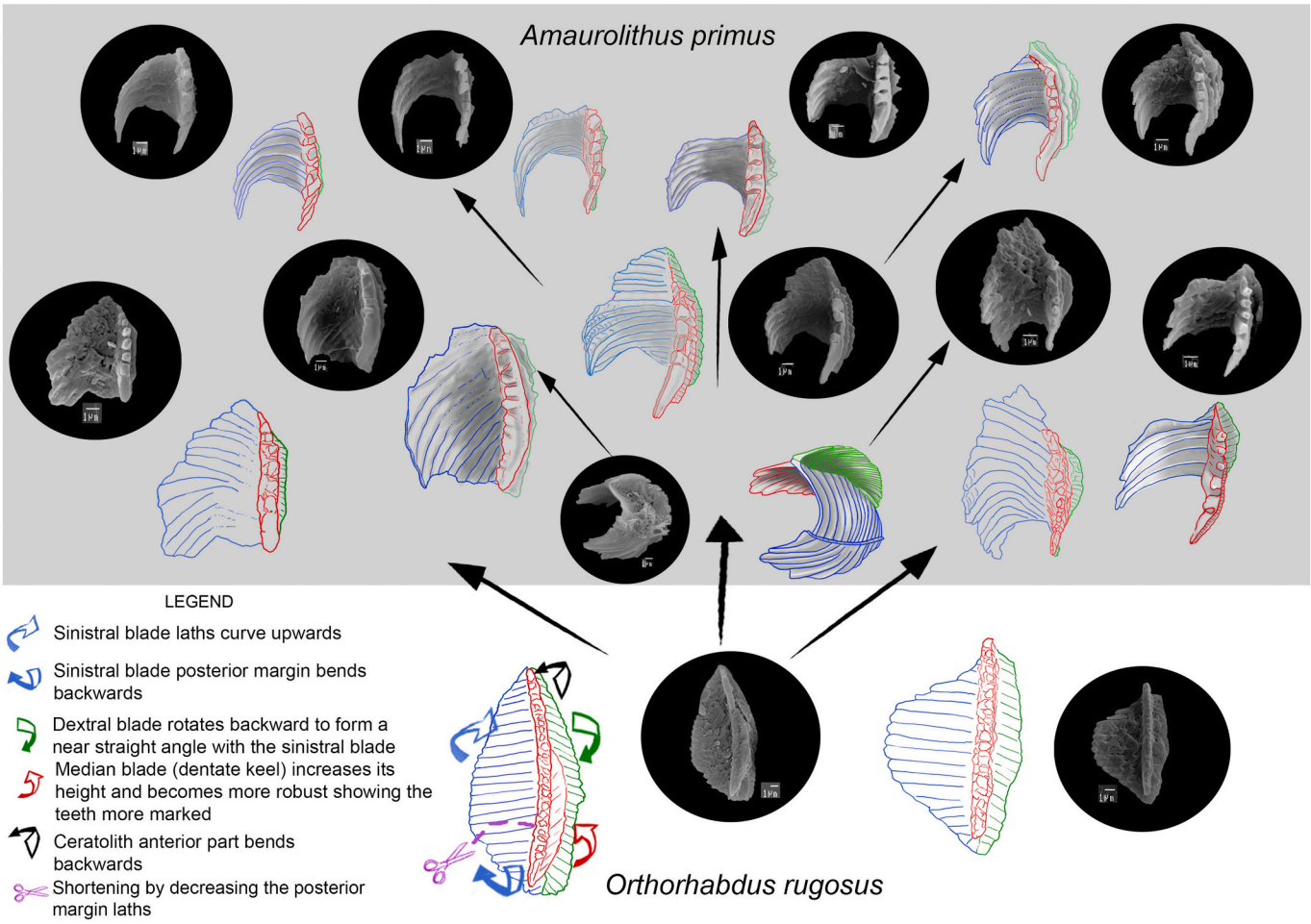


**Fig. 5.** Sketch of the morphological relationships between *A. primus* and *O. rugosus*. Colours mark different structures: Blue, sinistral blade/wing; Green, dextral blade/wing; Red, median blade/wing or the dentate keel. Modification on *O. rugosus*: Shortening of the specimen; Sinistral blade (blue): Lateral lengthening and its end portion curved upwards, concave to the observer; Dextral blade (green): Rotates backward; Median blade (red): Elevates and becomes more robust showing more marked teeth. (For interpretation of the references to colour in this figure legend, the reader is referred to the web version of this article.)

scarce. The most recent sample of *A. delicatus* is the 1237B 6H 4–75 (see Annex 1) calibrated by Tiedemann et al. (2007) to 2.93 Ma.

## 9. *Amaurolithus tricorniculatus* and *Amaurolithus ninae*

*Amaurolithus tricorniculatus* was established as a *comb. nov.* by Gartner and Bukry in 1975, modifying and extending the original definition of Gartner (1967) of *Ceratolithus tricorniculatus*, as a slightly asymmetrical horseshoe-shaped coccolith on which a pronounced apical spine is present on one side of the arch and more or less in line with the shorter of the two horns. Cross-polarised light may exhibit slight or no birefringence.

Based on our observations, we consider that the forms included in *A. tricorniculatus* correspond to two morphologies. One includes the original definition by Gartner (1967) as birefringent, appearing during the Early Pliocene, and the other observed during the Messinian, not birefringent (Rio et al., 1990), being forms of *A. primus* with the dextral wing most prominent in the anterior part, as an apical spine (characterised by a more developed apical region, Fig. 6M–O) or *A. delicatus* when there are forms less robust with an apical spine (Fig. 9D–F). Following the criteria of Raffi et al. (1998), we considered the non-birefringent forms of *A. tricorniculatus* to be morphovariants of *A. primus* or *A. delicatus*.

The morphotype *Amaurolithus ninae* (Perch-Nielsen, 1977) is generally a robust form of *A. delicatus* with a pronounced spur (Fig. 9K and N). Following the criteria of Raffi et al. (1998), we considered *A. ninae* to be a morphovariant of *A. delicatus*, characterised by a more developed apical region.

## 10. Origin of *Nicklithus amplificus*

The first record of *N. amplificus* was observed in samples 999A 23 × 3 W-80 (6.985 Ma) and 1237B 14H 3 W-95. The initial forms were triangular and quite robust, showing all the characteristics of the species (Fig. 10 and 11A–C), and usually had broken beaks or hooks (Fig. 4 H–O). They have been named integrade (Rio et al., 1990; Raffi and Flores, 1995) or crossover forms (Raffi et al., 2006). *Nicklithus amplificus* with well-developed beaks or hooks (Fig. 10 and 11G) was found in the most recent samples 999A 23×-2 W-40 (dated at 6.942 Ma) and 1237B 14H 1 W-95. Herein, we consider a new Lowest Occurrence (LO) when the triangular robust forms appear. As is the case with *A. primus*, it showed a stylisation trend over time.

Gartner and Bukry (1975) established *A. primus* as the ancestor of robust forms of *A. amplificus*. Blair et al. (2017) also considered *A. amplificus* to be derived from *A. primus;* however, our observations in the studied samples are consistent with the conclusion of Raffi et al. (1998) that *Nicklithus amplificus* evolved directly from *O. rugosus*, naming the new genus *Nicklithus* within the family. Fig. 10 illustrates the modifications of *O. rugosus* specimens to produce *Nicklithus amplificus* forms.

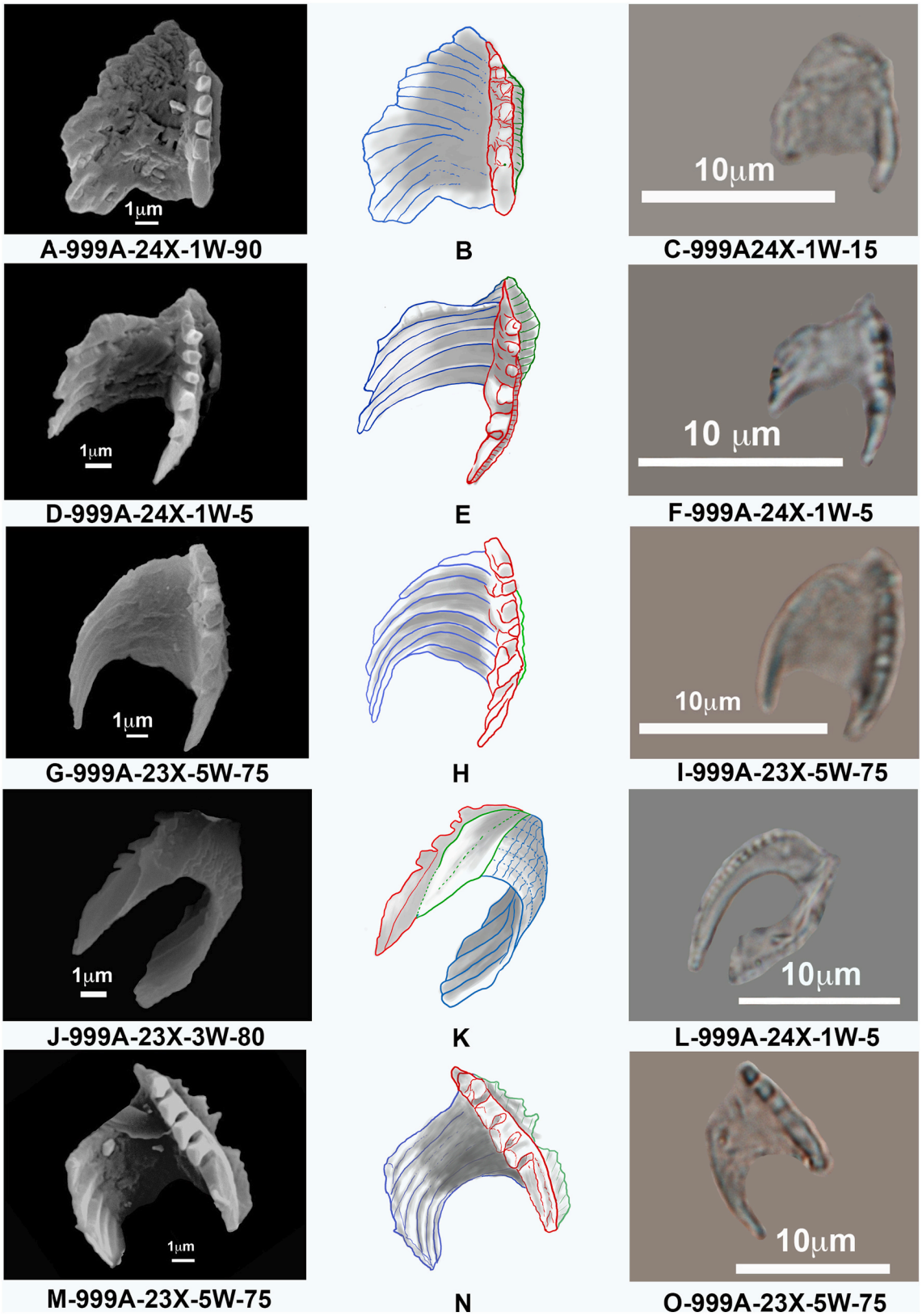


**Fig. 6.** Morphological variability in *A. primus*. A-F: Early *A. primus* during the end of the Tortonian-Early Messinian. A, D, G, and M: *A. primus* (ufv, SEM); B, E, H and N: Drawn after the picture shown in A, D, G, and M respectively; C, F, I, and O: *A. primus* (ufv) comparable to A, D, G, and M, respectively (PM, PN); J: *A. primus* (bfv, SEM); K: Drawn after the picture shown in J; L: *A. primus* (bfv) comparable to J (PM, PN).

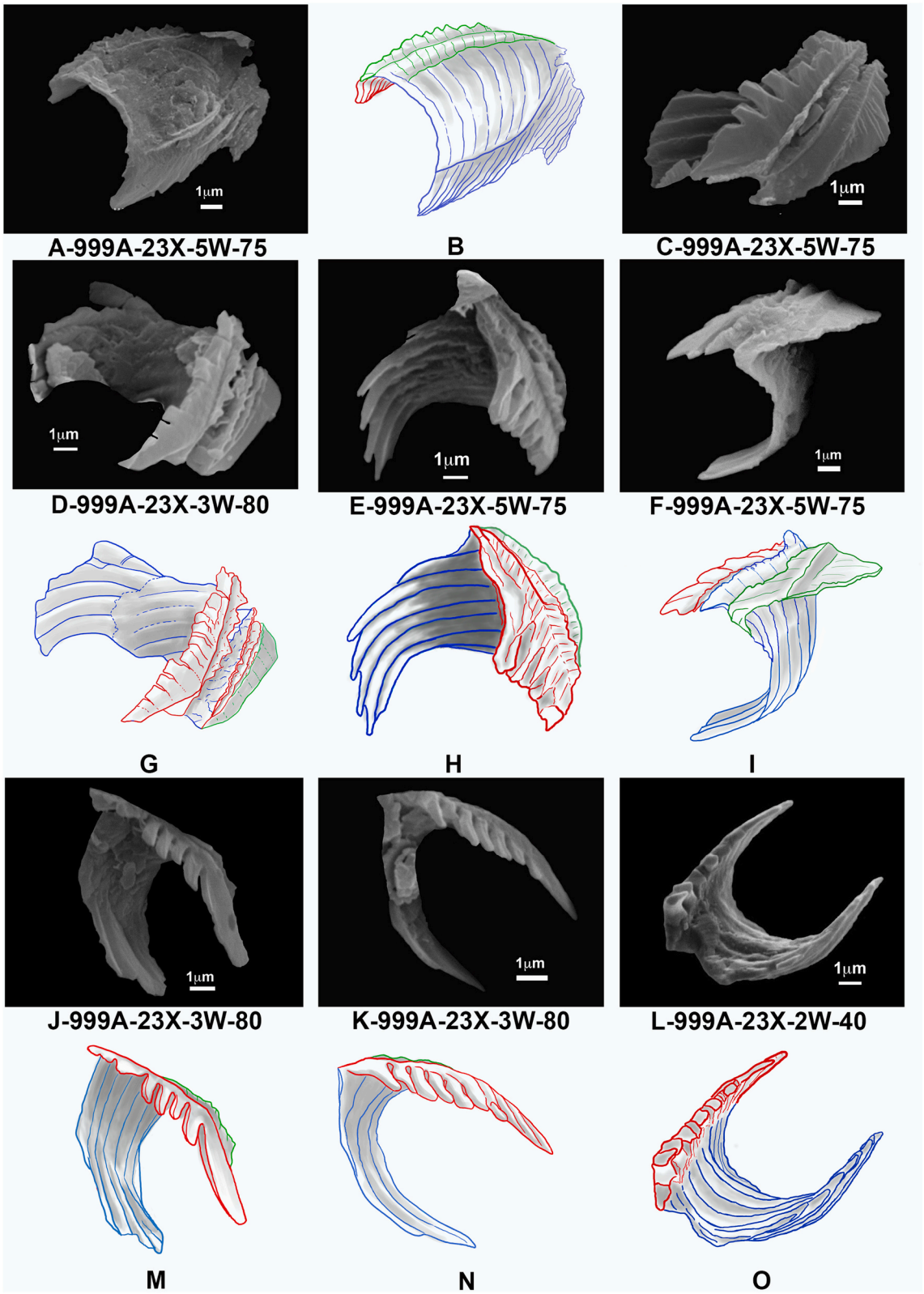


**Fig. 7.** Morphological variability of *A. primus*. A: *A. primus* (bfv, SEM); B: Drawn after the picture shown to the right; C: *A. primus* (SEM) in side view partially broken; D: *A. primus* lateral ufv (SEM) partially broken showing its wings separately; G: Drawn after the picture shown in D; E: *A. primus* (ufv) robust form (SEM); H: Drawn after the picture shown in E; F: *A. primus* posterior view (SEM) showing its wings; I: Drawn after the picture shown in F; J, K, and L: *A. primus* (ufv) elongated and stylised forms (SEM); M, N, and O: Drawn after the pictures shown in J, K, and L, respectively.

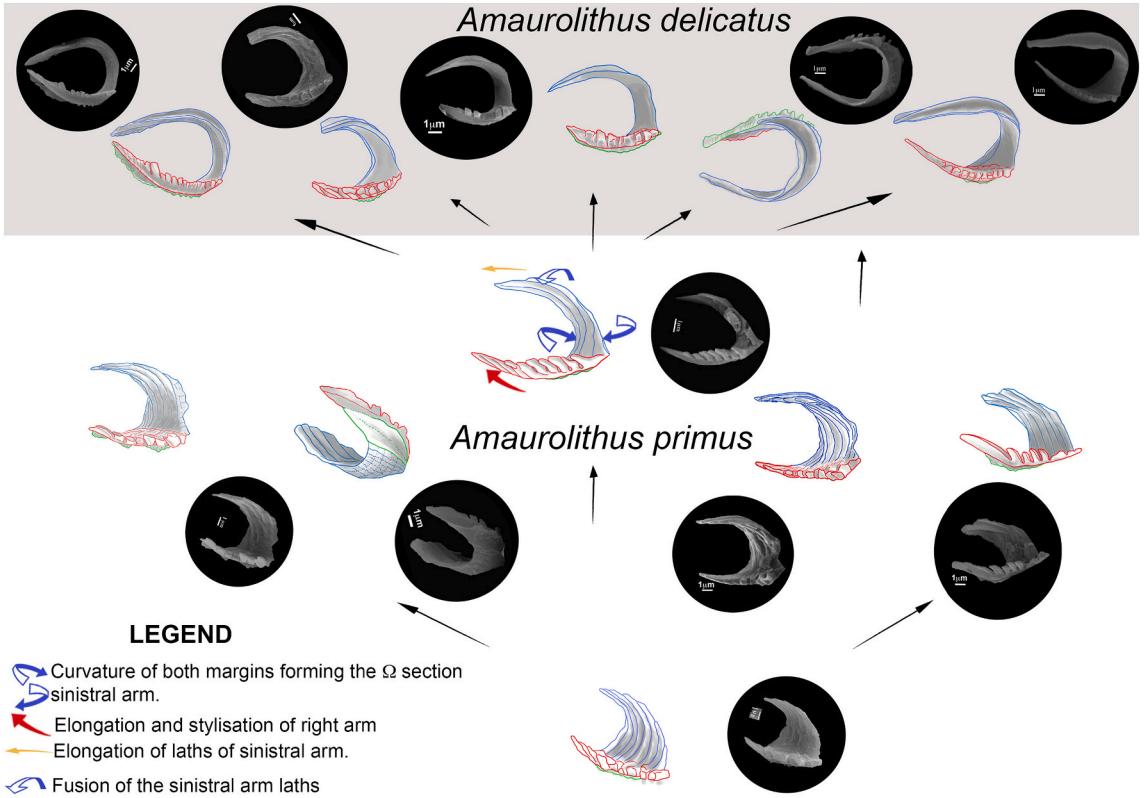


**Fig. 8.** Morphological changes producing *A. delicatus* evolving from *A. primus*. Morphological changes: Sinistral wing (blue): elongation, lath fusion, width reduction, thickness decrease, and development of a flattened omega (Ω) section. Dentate keel (red): elevated, elongated, and stylised. Dextral wing (green): reduced, stylised, and prolongated forming a posterior velum. (For interpretation of the references to colour in this figure legend, the reader is referred to the web version of this article.)

The sudden appearance of the fossil record of *N. amplificus* coexisting with the *O. rugosus* ancestor without intermediate forms suggests that the changes occurred at the same time, as is the case in the origin of *A. primus* and *A. delicatus* (Fig. 10).

Fig. 11 illustrates the variability in the form of *N. amplificus*. The intergrade forms [as mentioned by Raffi et al., 1998] observed in the PM (Figs. 4J–O and 11A–C) were interpreted as intermediate forms between *O. rugosus* and *N. amplificus* or the morphovariant *O. extensus*. However, when observed with SEM, these robust specimens were either broken *O. rugosus* or triangular-shaped initial forms of *N. amplificus*, and even though they were more robust, they already had all the features of the species (Fig. 11A–C).

The last occurrence of *N. amplificus* was in samples 999A 20H 3–70 (6.049 Ma) and 1237B 12H-3-75.

## 11. Discussion

The origin and evolutionary tendencies of the genera *Amaurolithus* (two species) and *Nicklithus* were analysed based on the morphological features of the nannoliths preserved within the sedimentary record. Raffi et al. (1998) described a sequence of gradual modifications of *O. rugosus* would produce, at three different time points, after a series of intermediate forms, *A. primus*, *N. amplificus*, and *C. acutus*. They also described specimens as *O. extensus* and *O. finifer* morphovariants (Theodoridis, 1984) together with the intermediate forms, observed just below and across the appearance levels of *A. primus*, *N. amplificus*, and *C. acutus*. The appearance of intermediate forms, described by Raffi et al. (1998), in which 'transition takes place during a period of about 160 kyr to 20 kyr', would highlight sequences with small morphological changes that accumulate with time.

Figures of our work illustrate observations of SEM and PM images that the morphologies initially assigned with the PM to *O. extensus* and/or intermediate forms between *O. rugosus* and *A. primus* (see Raffi et al., 1998 and Figs. 4 and 6), when compared with equivalent SEM images, are broken specimens of *O. rugosus* or initial forms of *A. primus*.

The initial specimens of *A. primus* were considered intermediate forms (intergrade forms) of *O. rugosus-A. primus*, because they have robust morphologies that preserve many characteristics of their ancestors. All characteristics that define the species were present in all observed individuals (Figs. 5 and 6). However, we did not obtain SEM images in which the evolutionary modification sequence was revealed. It could be argued that a tighter sampling could detect such a sequence but given the number and separation of SEM samples for the time interval considered, it would be surprising not to find these intermediate forms (extending for approximately 100 kyr), even if only by mere chance.

The same can be said with respect to the SEM and PM observations of the evolutionary origin of *N. amplificus* from *O. rugosus* (Fig. 10), where no changes in sequence can be detected. Non-intermediate forms were observed in the link between *A. delicatus* and *A. primus* (Fig. 8). There were small changes, but as they were presented together and at the same time, a new species can be established from the beginning. The initial forms of the new species are also maintained over time, and new diverse specimens with more stylised morphologies are produced before becoming extinct (Fig. 9).

The observed data suggest that the evolutionary origin of *A. primus, A. delicatus*, and *N. amplificus* does not seem to adjust to a gradualist pattern of evolution and speciation, but to a sudden and repeated appearance at different times (two for the *Amaurolithus* and one for *Nicklithus* genera) during the Late Miocene, forms already having the typical morphological characteristics that define the species. It would most likely be a case of punctuational pattern of speciation with a long-

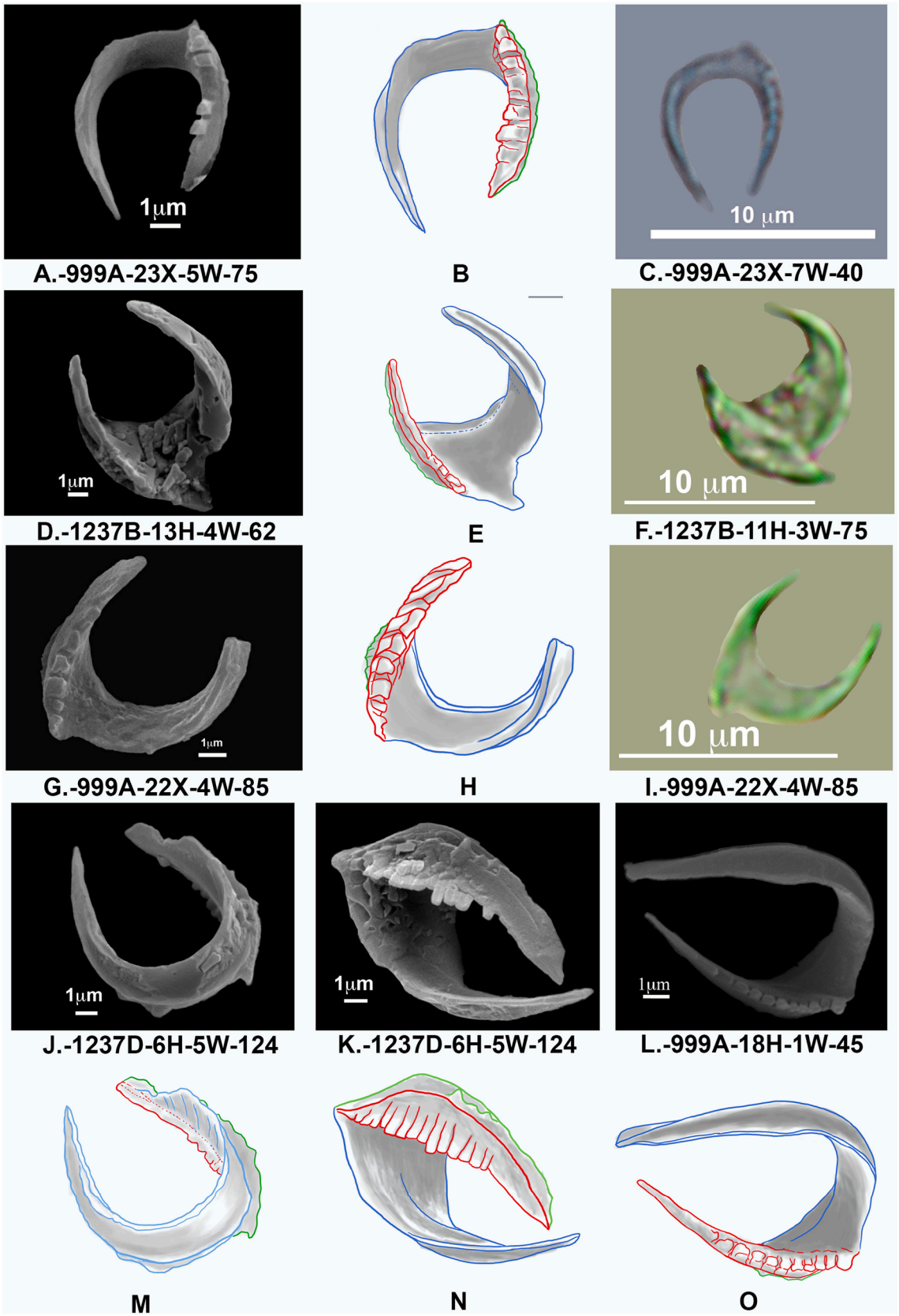


**Fig. 9.** Morphological variability of *A. delicatus*. A: *A. delicatus* (ufv) initial specimen (SEM); B: Drawn after the picture shown to the left; C: *A. delicatus* (ufv) equivalent to A (PM, PN); D: *A. delicatus* (ufv) morphology sometimes assigned to *A. tricorniculatus* (SEM); E: Drawn after the picture shown to the left; F: *A. delicatus* (ufv) equivalent from D (PM, PN). G: *A. delicatus* (ufv) morphology commonly assigned to *A. primus* (SEM); H: Drawn after the picture shown to the left; I: *A. delicatus* (ufv) equivalent from G (PM, PN); J: *A. delicatus* (bfv, SEM); M: Drawn after the picture shown in J; K: *A. delicatus* lateral ufv morphology commonly assigned to *A. ninae* (SEM); N: Drawn after the picture shown in K; L: *A. delicatus* lateral ufv (SEM); O: Drawn after the pictures shown in L.

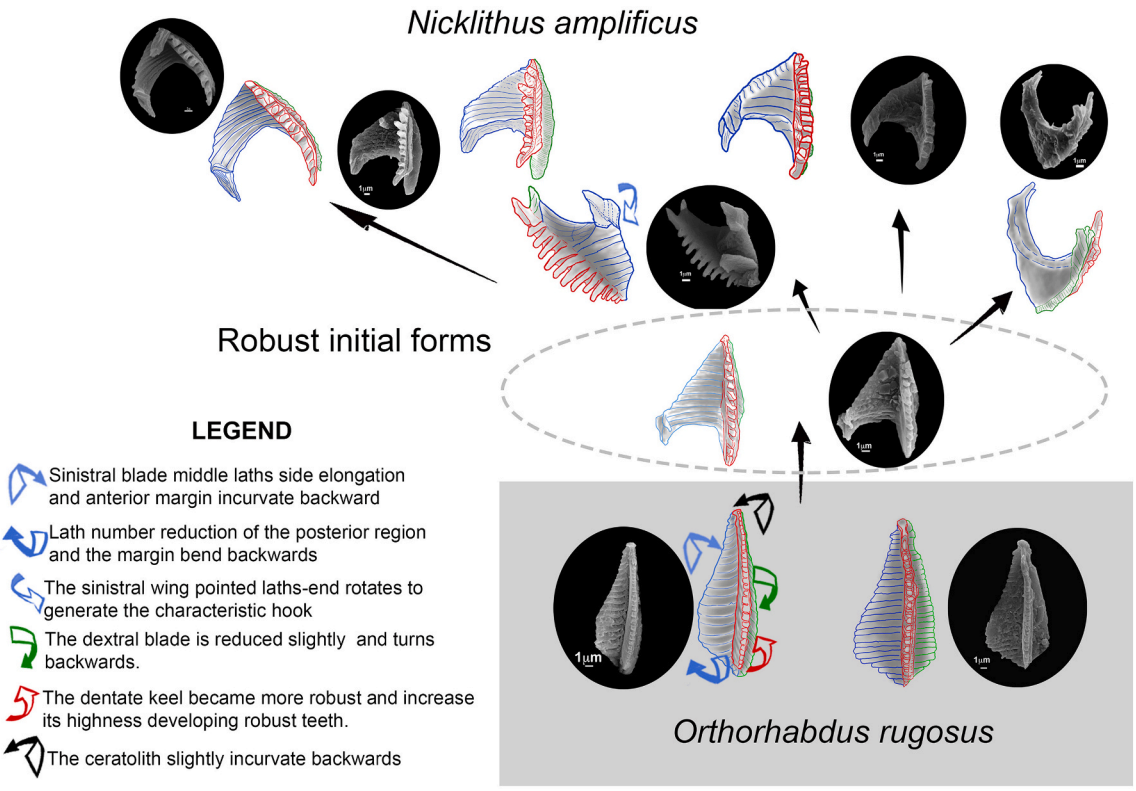


**Fig. 10.** Modification of the structure of *O. rugosus* to reach forms identifiable with *Nicklithus amplificus*. Morphological changes: Sinistral blade (blue) side elongation, forming the arch and development of the characteristic hook (or beak); Dextral blade (green); the median blade (dentate keel, red) became more robust. The posterior end separates from the dextral wing producing a characteristic V-end on the left arm. The ceratolith becomes shorter. The changes are not arranged as a phyletic sequence. (For interpretation of the references to colour in this figure legend, the reader is referred to the web version of this article.)

term stasis period in which *O. rugosus*, although it has an important variability, does not seem to show any notable morphological change. Although remarkable genetic changes may occur without expressing themselves (manifest) as morphological changes (cryptic speciation) (Saez et al., 2003), in particular moments (favourable conditions), they can be expressed as a result of the selection of those morphological modifications generated as a result of the set of genetic changes that would lead to an evolutionary advantage.

The Late Miocene, particularly during the Messinian, can be associated with the main geologic events causing changes in global oceanic and atmospheric circulation (Vidal et al., 2002) and starting modern deep water circulation (Nisancioglu, 2003). This high instability period would generate oceanic compartments, which undoubtedly favour the appearance of new ecological niches in nearby and similar habitats, favouring speciation processes that select morphological innovations, generating changes, and substituting species with better adapted ones.

The stasis period of *O. rugosus* is punctuated by two periods of rapid speciation, producing first *A. primus* around 7.354 Ma, from which *A. delicatus* was derived around 7.226 Ma, and later *N. amplificus* at approximately 6.985 Ma. These initial forms will subsequently undergo an important variability with a stylisation trend that cannot be considered as the genesis of new species, because the degree of morphological change observed would fall within the typical variability of the species. It should also be noted that the continuity of the *O. rugosus* ancestral species produced the *Ceratolithus*-branch at the end of the Messinian.

Natural selection fixes more favourable traits, by geographic isolation (allopatric speciation) or ecologic isolation (sympatric speciation). Allopatric speciation is typically considered the dominant geographic mode of speciation; however, there is growing theoretical and empirical support for sympatric speciation (Dieckmann and Doebei, 1999; Crow et al., 2010). In the marine realm, the primacy of allopatric speciation has long been questioned owing to the relatively large range and high dispersal potential of marine species (Palumbi, 2004). Since Maynard Smith (1966), many models have been used to describe the conditions under which sympatric speciation is theoretically possible (Dickinson and Antonovics, 1973; Diehl and Bush, 1989). The usual approach is to assume that there is disruptive selection in a polymorphic population with assortative mating.

The evolutionary origin of *Amaurolithus* and *Nicklithus* is more similar to a sympatric speciation model because no evidence of the spatial isolation of *O. rugosus* populations has been obtained. Examples of this in different groups of organisms have been reported by Schliewen et al. (2001), Barluenga et al. (2006), De Vargas et al. (1999), and Lazarus et al. (1995). In the case of coccolithophores such as *Coccolithus pelagicus*, there is clear evidence that the two subspecies occupy different geographic ranges, suggesting that allopatric speciation has occurred; for *C. leptoporus*, there is no evidence of present or past spatial isolation of populations, suggesting sympatric speciation (Geisen et al., 2002).

*Orthorhabdus rugosus*, *A. primus*, *A. delicatus*, and *N. amplificus* are single calcite elements with the crystallographic c-axis perpendicular to the length of the nannolith (ortholith/ceratolith), showing non-birefringence or only weak birefringence, as the c-axis is usually oriented perpendicular or nearly perpendicular to the horseshoe-preferred orientation. In the four nannoliths, the only blade/wing that remains almost unchanged is the median one, always oriented upwards in the upper face view, so it may be considered that the c-axis is subparallel to this blade. This has an interesting implication, as if the median blades/wings mark the crystallography of a single calcite crystal, this could be considered the initial point in the nucleation process.

## 12. Conclusions

The abundant and diverse Ceratholithaceae assemblages from the Upper Miocene sediments obtained from the Equatorial Pacific and

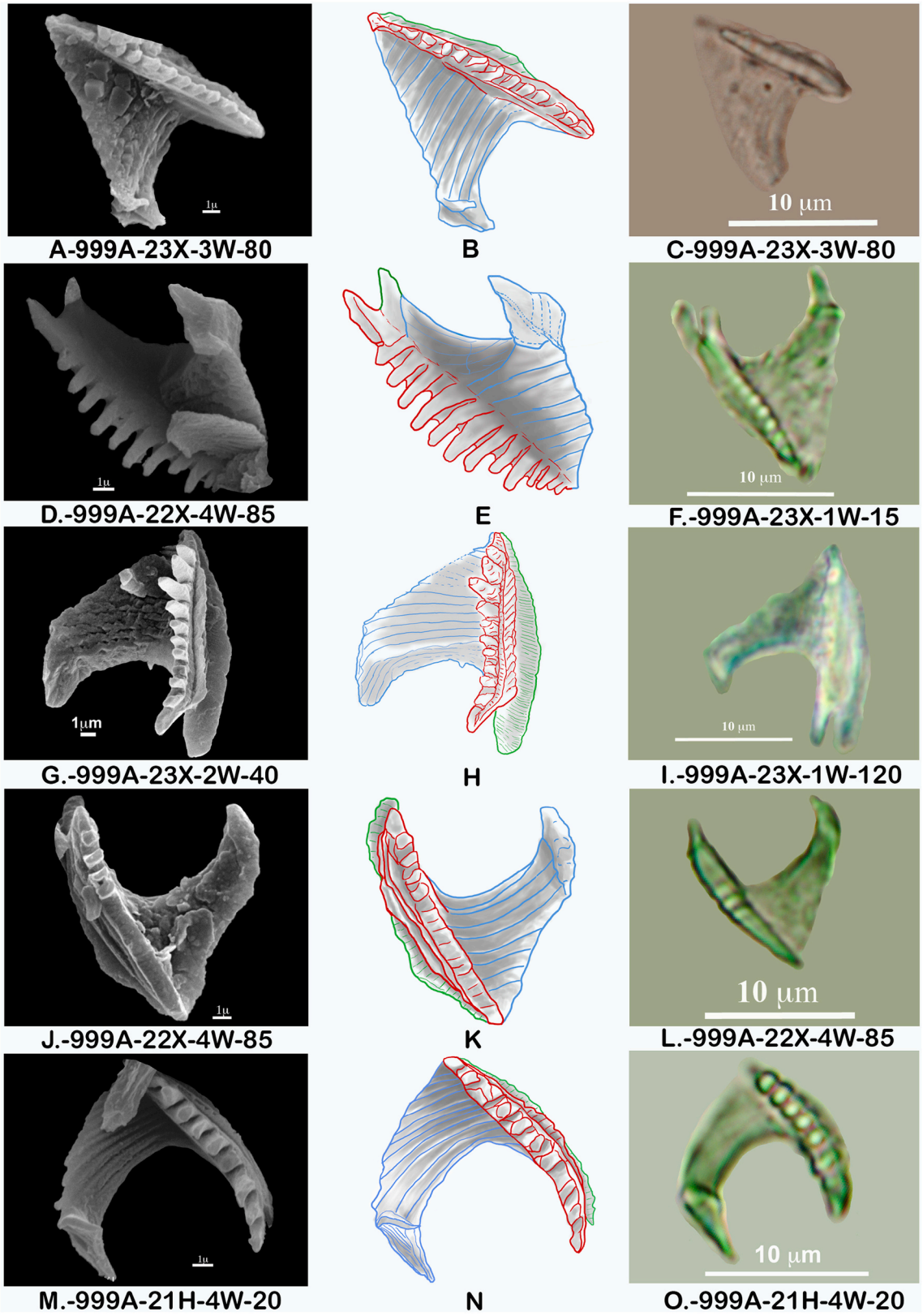


**Fig. 11.** Morphological variability of *N. amplificus* during the Messinian. A: Early *N. amplificus* ufv commonly classified as 'integrade' *O. rugosus- N. amplificus* obtained by SEM; B: Drawn after the picture shown to the left; C: Early *N. amplificus* ufv commonly classified as 'integrade' *O. rugosus-N. amplificus* (PM, PN); D: *N. amplificus* lateral ufv (SEM); E: Drawn after the picture shown in D; F: *N. amplificus* ufv equivalent from D (PM, PN); G, J, and M: *N. amplificus* ufv (SEM); H, K, and N: Drawn after the picture shown to the left; I, L, and O: *N. amplificus* ufv equivalent from G, J, and M, respectively (PM, PN).

Caribbean Sea at Site 1237 and Hole 999A during the time interval between 7.400 Ma and 6.049 Ma offered an opportunity to observe evolutionary processes within the genera *Orthorhabdus, Amaurolithus*, and *Nicklithus*.

Detailed SEM images of well-preserved specimens allowed us to establish phylogenetic relationships between the genera *Orthorhabdus* and *Amaurolithus* and *Orthorhabdus* and *Nicklithus* to document speciation.

This study describes detailed morphological changes that generated the new species *A. primus* from its predecessor *O. rugosus* at 7.354 Ma, the first *A. delicatus* derived from *A. primus* at 7.226 Ma, and *N. amplificus* originating from *O. rugosus* at 6.985 Ma.

The new ceratolith species that originated from rapid changes did not respond to a gradualist pattern of evolution and speciation, but rather to a punctuational pattern of speciation with one long-term stasis period in which the only existing species, *O. rugosus*, did not undergo any appreciable morphological change, although remarkable genetic changes may occur (cryptic speciation).

Two periods of rapid speciation produced *A. primus*, from which *A. delicatus* was derived, and finally *N. amplificus*, in a clear example of iterative evolution without the extinction of the ancestor species.

The appearance of *A. delicatus* was rapid, following a continuous evolutionary trend that displays gradual morphological changes without lineage division (e.g. phyletic gradualism or gradual evolution), which has been attributed to a lack of barriers to gene flow in species that are both cosmopolitan and phenotypically plastic (Benton and Pearson, 2001).

New time ranges for *A. primus* (7.354–6.282 Ma) and *Nicklithus amplificus* (6.985–6.049 Ma) are documented. The sudden evolutionary appearance of the studied species, as well as the calibration of the appearance and extinction events, is of special utility in the biostratigraphy of the Messinian.

## Declaration of Competing Interest

Jéose-Enrique Tent-Manclus reports was provided by Spain Ministry of Science and Innovation. José-Abel Flores reports was provided by Spain Ministry of Science and Innovation. José-Enrique Tent-Manclús reports was provided by Generalitat Valenciana Presidencia.

## Acknowledgements

This work was supported by projects RTI2018-099489-B-I00 and PID2020-114381GB-I00 (spanish Ministry of Science, Innovation and Universities). The authors would like to thank A. Estévez for his comments on the early drafts of the paper and Verónica López, and Andrés Amorós of the Microscopy unit of the Alicante University for their assistance. This study was funded by the European Union NextGenerationEU project GVA-THINKINAZUL/2021/039. We also thank the reviewer and journal editor for their support and constructive reviews. This study used samples provided by the Ocean Drilling Program (ODP).

## Appendix A. Supplementary data

Supplementary data to this article can be found online at https://doi.org/10.1016/j.marmicro.2022.102156.

## References

Alcober, J., Jordan, R.W., 1997. An interesting association between *Neosphaera coccolithomorpha* and *Ceratolithus cristatus* (Haptophyta). Eur. J. Phycol. 32, 91–93. https://doi.org/10.1080/09541449710001719385.

Aubry, M.-P., 1988. Handbook of Cenozoic Calcareous Nannoplankton. Book 2: Ortholithae (Catinasters, Ceratoliths, Rhabdoliths). Micropaleontology Press (279 pp.).

Barluenga, M., Stölting, K.N., Salzburger, W., Muschick, M., Meyer, A., 2006. Sympatric speciation in Nicaraguan crater lake cichlid fish. Nature 439, 719–723.

Benton, M.J., Pearson, P.N., 2001. Speciation in the fossil record. Trends Ecol. Evol. 16, 405–411.

Bergen, J., De Kaenel, E., Blair, S., Boesiger, T., Browning, E., 2017. Oligocene-Pliocene taxonomy and stratigraphy of the genus *Sphenolithus* in the circum North Atlantic Basin: Gulf of Mexico and ODP Leg 154. J. Nannoplankton Res. 37, 77–112.

Bickert, T., Haug, G.H., Tiedemann, R., 2004. Late Neogene benthic stable isotope record of Ocean Drilling Program Site 999: Implications for Caribbean paleoceanography, organic carbon burial, and the Messinian Salinity Crisis. Paleoceanography 19, PA1023. https://doi.org/10.1029/2002PA000799.

Blair, S., Bergen, J., de Kaenel, E., Browning, E., Boesiger, T., 2017. Upper Miocene -lower Pliocene taxonomy and stratigraphy of the circum North Atlantic Basin: radiation and extinction of Amauroliths, Ceratoliths and the *D. quinqueramus* lineage. J. Nannoplankton Res. 37, 113–144.

Blaj, T., Henderiks, J., Young, J.R., Rehnberg, E., 2010. The Oligocene nannolith *Sphenolithus* evolutionary lineage: Morphometrical insights from the palaeo-equatorial Pacific Ocean. J. Micropalaeontol. 29, 17–35. https://doi.org/10.1144/jm.29.1.17.

Boesiger, T., De Kaenel, E., Berger, J., Browning, E., Blair, S., 2017. Oligocene to Pleistocene taxonomy and stratigraphy of the genus *Helicosphaera* and other placolith taxa in the circum North Atlantic Basin. J. Nannoplankton Res. 37, 145–175.

Bord, D., 2013. Microevolution in Coccolithophores. Rutgers University. https://doi.org/10.7282/T3639MRQ.

Browning, E., Berger, J., Blair, S., Boesiger, T., De Kaenel, E., 2017. Late Miocene to late Pliocene taxonomy and stratigraphy of the genus *Discoaster* in the circum North Atlantic Basin: Gulf of Mexico and ODP Leg 154. J. Nannoplankton Res. 37, 189–214.

Buitrago-Reina, Y.M., Flores, J., Sierro, F.J., 2010. Calcareous nannofossils Upper Miocene biostratigraphy and biochronology at western equatorial Atlantic (ODP Site 999). Rev. Esp. Micropaleontol. 42, 301–319.

Bukry, D., 1971. *Discoaster* evolutionary trends. Micropaleontol. 17, 43–52.

Bukry, D., 1979. Neogene coccolith stratigraphy, Mid-Atlantic Ridge, Deep Sea Drilling Project Leg 45. Init. Rep. Deep Sea Drill. Proj. Leg 45, 307–317. https://doi.org/10.2973/dsdp.proc.45.109.1979.

Ciummelli, M., Raffi, I., 2013. New data on the stratigraphic distribution of the nannofossil genus *Catinaster* and on evolutionary relationships among its species. J. Micropalaeontol. 32, 197–205. https://doi.org/10.1144/jmpaleo2013-002.

Cros, L., Kleijne, A., Zeltner, A., Billard, C., Young, J.R., 2000. New examples of holococcolith–heterococcolith combination coccospheres and their implications for coccolithophorid biology. Mar. Micropaleontol. 39, 1–34. https://doi.org/10.1016/S0377-8398(00)00010-4.

Crow, K.D., Munehara, H., Bernardi, G., 2010. Sympatric speciation in a genus of marine reef fishes. Mol. Ecol. 19, 2089–2105.

De Kaenel, E., Berger, J., Browning, E., Blair, S., Boesiger, T., 2017. Uppermost Oligocene to Middle Miocene *Discoaster* and *Catinaster* taxonomy and stratigraphy in the circum North Atlantic Basin: Gulf of Mexico and ODP Leg 154. J. Nannoplankton Res. 37, 215–244.

De Vargas, C., Norris, R., Zaninetti, L., Gibb, S.W., Pawlowski, J., 1999. Molecular evidence of cryptic speciation in planktonic foraminifers and their relation to oceanic provinces. PNAS 96 (6), 2864–2868.

Dickinson, H., Antonovics, J., 1973. Theoretical considerations of sympatric divergence. Am. Nat. 107, 256–274.

Dieckmann, U., Doebei, M., 1999. On the origin of species by sympatric speciation. Nature 400, 354–357. https://doi.org/10.1038/22521.

Diehl, S.R., Bush, G.L., 1989. The role of habitat preference in adaptation and speciation. In: Otte, D., Endler, J.A. (Eds.), Speciation and its Consequences. Sinauer, Sunderland, Massachusetts, pp. 345–365.

Flores, J.A., Sierro, F.J., 1997. Revised technique for calculation of calcareous nannofossil accumulation rates. Micropaleontology 43, 321–324.

Gartner, S., 1967. Calcareous nannofossils from Neogene of Trinidad, Jamaica, and Gulf of Mexico. Univ. Kansas Paleontol. Contr. Pap. 29, 1–7.

Gartner, S., Bukry, D., 1975. Morphology and phylogeny of the coccolithophycean family Ceratolithaceae. J. Res. US Geol. Surv. 3, 451–465.

Geisen, M., Billard, C., Broerse, A.T.C., Cros, L., Probert, I., Young, J.R., 2002. Life-cycle associations involving pairs of holococcolithophorid species: intraspecific variation or cryptic speciation? Eur. J. Phycol. 37, 531–550. https://doi.org/10.1017/S0967026202003852.

Gradstein, F.M., Ogg, J.G., Schmitz, M.D., Ogg, G.M., 2012. The Geologic Time Scale 2012. Cambridge University Press. https://doi.org/10.1016/B978-0-444-59425-9.01001-5.

Haq, B.U., 1973. Evolutionary Trends in the Cenozoic Coccolithophore Genus *Helicopontosphaera*. Micropaleontology 19, 32–55.

Jordan, R.W., Chamberlain, A.H.L., 1997. Biodiversity among haptophyte algae. Biodivers. Conserv. 6, 131–152.

Kameo, K., Bralower, T.J., 2000. Neogene calcareous nannofossil biostratigraphy of Sites 998, 999, and 1000, Caribbean Sea. In: Leckie, R.M., Sigurdsson, H., Acton, G.D., Draper, G. (Eds.), Proc. ODP, 165 Sci. Results. College Station, TX (Ocean Drilling Program), pp. 3–17.

Kamptner, E., 1950. Über den submikroskopischen Aufbau der Coccolithen. Anz. Österr. Akad. Wiss. Math.-Naturw. Kl. 87, 152–158.

Kamptner, E., 1954. Untersuchungen ueber den Feinbau der Coccolithen. Arch. Protistenkd. 100, 1–90.

Lancis, C., 1998. El nanoplancton calcáreo de las cuencas béticas orientales. PhD Thesis. University of Alicante.

Lazarus, D., Hilbrecht, H., Spencer-Cervato, C., Thierstein, H.R., 1995. Sympatric speciation and phyletic change in *Globorotalia truncatulinoides*. Paleobiology 21, 28–51.

Lourens, L., Hilgen, F., Shackleton, N.J., Laskar, J., Wilson, D., 2004. The Neogene period. In: Gradstein, F.M., Ogg, J.G., Smith, A.G. (Eds.), A geologic Time Scale. Cambridge University Press, pp. 409–440.

Maynard Smith, J., 1966. Sympatric speciation. Am. Nat. 100 (916), 637–650.

Mix, A.C., Tiedemann, R., Blum, et al., 2003. Leg 202 summary. In: Mix, A.C., Tiedemann, R., Blum, P., et al. (Eds.), Proc. ODP, 202 Init. Reports. College Station, TX (Ocean Drilling Program), pp. 1–145.

Monechi, S., Reale, V., Bernaola, G., Balestra, B., 2013. The Danian/Selandian boundary at Site 1262 (South Atlantic) and in the Tethyan region: Biomagnetostratigraphy, evolutionary trends in fasciculiths and environmental effects of the Latest Danian Event. Mar. Micropaleontol. 98, 28–40. https://doi.org/10.1016/j.marmicro.2012.11.002.

Nisancioglu, K.H., 2003. Reorganization of Miocene deep water circulation in response to the shoaling of the central American Seaway. Paleoceanography 18, 1–12. https://doi.org/10.1029/2002PA000767.

Norris, R.E., 1965. Living cells of *Ceratolithus cristatus* (Coccolithophorineae). Arch. Protistenkd. 108, 19–21.

Palumbi, S.R., 2004. Marine reserves and ocean neighborhoods: the spatial scale of marine populations and their management. Annu. Rev. Environ. Resour. 29, 31–68.

Perch-Nielsen, K., 1977. Albian to Pleistocene calcareous nannofossils from the western South Atlantic, DSDP Leg 39. Init. Rep. Deep Sea Drill. Proj. Leg 39, 699–823. https://doi.org/10.2973/dsdp.proc.39.131.1977.

Perch-Nielsen, K., 1985. Cenozoic calcareous nannofossils. In: Bolli, H.M., Saunders, J.B., Perch-Nielsen, K. (Eds.), Plankton Stratigraphy. Cambridge Univ. Press, Cambridge, pp. 27–553.

Raffi, I., Flores, J.A., 1995. Pleistocene through Miocene calcareous nannofossils from eastern equatorial Pacific Ocean (Leg 138). In: Pisias, N.G., Mayer, L.A., Janecek, T. R., Palmer-Julson, A., van Andel, T.H. (Eds.), Proc. ODP, Sci. Results 138, Coll. Station. TX (Ocean Drilling Program), pp. 233–286. https://doi.org/10.2973/odp.proc.sr.138.112.1995.

Raffi, I., Backman, J., Rio, D., 1998. Evolutionary trends of tropical calcareous nannofossils in the late Neogene. Mar. Micropaleontol. 35 (1), 17–41. https://doi.org/10.1016/S0377-8398(98)00014-0.

Raffi, I., Backman, J., Fornaciari, E., Pälike, H., Rio, D., Lourens, L., Hilgen, F., 2006. A review of calcareous nannofossil astrobiochronology encompassing the past 25 million years. Quat. Sci. Rev. 25, 3113–3137. https://doi.org/10.1016/j.quascirev.2006.07.007.

Rio, D., Fornaciari, E., Raffi, I., 1990. Late Oligocene through early Pleistocene calcareous nannofossils from western equatorial Indian Ocean (Leg 115). In: Duncan, R.A., Backman, J., Peterson, L.C., et al. (Eds.), Proc. ODP, Sci. Results 115, Coll. Station. TX (Ocean Drill. Program), pp. 175–235. https://doi.org/10.2973/odp.proc.sr.115.152.1990.

Romein, A.J.T., 1979. Lineages inthe Early Paleogene calcareous nannoplankton. Utrecht Micropaleontol. Bull. 22, 231.

Saez, A.G., Probert, I., Geisen, M., Quinn, P., Young, J.R., Medlin, L.K., 2003. Pseudo-cryptic speciation in coccolithophores. PNAS 100, 7163–7168. https://doi.org/10.1073/pnas.1132069100.

Schliewen, U., Rassmann, K., Markmann, M., Markert, J., Kocher, T., Tautz, D., 2001. Genetic and ecological divergence of a monophyletic cichlid species pair under fully sympatric conditions in Lake Ejagham. Cameroon. Mol. Ecol. 10 (6), 1471–1488.

Sigurdsson, H., Leckie, R.M., Acton, G.D., et al., 1997. 4. Site 999. In: Sigurdsson, H., Leckie, R.M., Acton, G.D., et al. (Eds.), Proc. ODP, Init. Reports. 165, Coll. Station. TX (Ocean Drill. Program), pp. 131–230. https://doi.org/10.2973/odp.proc.ir.165.104.1997.

Sprengel, C., Young, J.R., 2000. First direct documentation of associations of *Ceratolithus cristatus* ceratoliths, hoop-coccoliths and *Neosphaera coccolithomorpha* planoliths. Mar. Micropaleontol. 39, 39–41. https://doi.org/10.1016/S0377-8398(00)00012-8.

Tappan, H., 1980. The Paleobiology of Plant Protists. W.H. Freeman, San Francisco, CA.

Theodoridis, S.A., 1984. Calcareous nannofosils biozonation of the Miocene and revision of the helicoliths and discoasters. Utrecht Micropaleontol. Bull. 32, 271.

Tiedemann, R., Mix, A., 2007. Leg 202 synthesis: Southeast Pacific paleoceanography. In: Tiedemann, R., Mix, A.C., Richter, C., Ruddiman, W.F. (Eds.), Proc. ODP, Sci. Results 202, Coll. Station. TX (Ocean Drill. Program), pp. 1–56. https://doi.org/10.2973/odp.proc.sr.202.201.2007.

Tiedemann, R., Sturm, A., Steph, S., Lund, S.P., Stoner, J.S., 2007. Astronomically calibrated timescale from 6 to 2.5 Ma and benthic isotope stratigraphies, Sites 1236, 1237, 1239, and 1241. In: Tiedemann, R., Mix, A.C., Richter, C., Ruddiman, W.F. (Eds.), Proc. Ocean Drill. Program, Sci. Results 202, Coll. Station. TX (Ocean Drill. Program), pp. 1–69. https://doi.org/10.2973/odp.proc.sr.202.210.2007.

Vidal, L., Bickert, T., Wefer, G., Ro, U., 2002. Late Miocene stable isotope stratigraphy of SE Atlantic ODP Site 1085: Relation to Messinian events. Mar. Geol. 180, 71–85.

Young, J.R., 1990. Size variation of Neogene *Reticulofenestra* coccoliths from Indian Ocean DSDP Cores. J. Micropalaeontol. 9, 71–85. https://doi.org/10.1144/jm.9.1.71.

Young, J.R., 1998. Neogene. In: Bown, P. (Ed.), Calcareous Nannofossil Biostratigraphy. British Micropalaeontological Society Publications Series. Chapman & Hall, London, pp. 225–265.

Young, J.R., Bown, P.R., 2014. Some emendments to calcareous nannoplankton taxonomy. J. Nannoplankton Res. 33 (1), 39–46.

Young, J.R., Bown, P.R., Lees, J.A. (Eds.), 2022. "Ceratolithaceae" Nannotax3 website. International Nannoplankton Association (Accessed 7-July-2022). http://ina.tmsoc.org/Nannotax3/link.php?taxon=Ceratolithaceae.

Young, J.R., Davis, S.A., Bown, P.R., Mann, S., 1999. Coccolith ultrastructure and biomineralisation. J. Struct. Biol. 126, 195–215. https://doi.org/10.1006/jsbi.1999.4132.

Young, J.R., Geisen, M., Cros, L., Kleijne, A., Probert, I., Ostergaard, J.B., 2003. A guide to extant coccolithophore taxonomy. J. Nannoplankton Res. (Special Issue) 1, 1–132.

Young, J.R., Geisen, M., Probert, I., 2005. A review of selected aspects of coccolithophore biology with implications for paleobiodiversity estimation. Micropaleontology 51, 267–288. https://doi.org/10.2113/gsmicropal.51.4.267.